Tanaka, T., Itoh, H., Doi, K., Fukunaga, Y., Hosoda, K., Shintani, M., Yamashita, J., Chun, T.-H., Inoue, M., Masatsugu, K., Sawada, N., Saito, T., Inoue, G., Nishimura, H., Yoshimasa, Y., Nakao, K., 1999. Down regulation of peroxisome proliferator-activated receptor gamma expression by inflammatory cytokines and its reversal by thiazolidinediones. Diabetologia 42, 702–710.

Tontonoz, P., Hu, E., Spiegelman, B.M., 1994. Stimulation of adipogenesis in fibroblasts by PPAR gamma 2, a lipid-activated transcription factor. Cell 79, 1147–1156.

Tontonoz, P., Nagy, L., Alvarez, J.G.A., Thomazy, V.A., Evans, R.M., 1998. PPARgamma promotes monocyte/macrophage differentiation and uptake of oxidized LDL. Cell 93, 241–252.

Zhu, L., Bisgaier, C.L., Aviram, M., Newton, R.S., 1999. 9-*Cis* retinoic acid induces monocytes chemoattractant protein-1 secretion in human monocytic THP-1 cells. Arterioscler. Thromb. Vasc. Biol. 19, 2105–2111.

Available online at www.sciencedirect.com
SCIENCE DIRECT®
Journal of Molecular and Cellular Cardiology 38 (2005) 185–192
Journal of Molecular and Cellular Cardiology
www.elsevier.com/locate/yjmcc

Original Article

Hypertrophic responses to cardiotrophin-1 are not mediated by STAT3, but via a MEK5-ERK5 pathway in cultured cardiomyocytes

Nobuki Takahashi [a], Yoshihiko Saito [b,*], Koichiro Kuwahara [a], Masaki Harada [a], Keiji Tanimoto [a], Yasuaki Nakagawa [a], Rika Kawakami [a], Michio Nakanishi [a], Shinji Yasuno [a], Satoru Usami [a], Akihiko Yoshimura [c], Kazuwa Nakao [a]

[a] *Department of Medicine and Clinical Science, Kyoto University Graduate School of Medicine, Kyoto, Japan*
[b] *First Department of Internal Medicine, Nara Medical University, 840 Shijo-cho, Kashihara-city, Nara 634-8522, Japan*
[c] *Division of Molecular and Cellular Immunology, Medical Institute of Bioregulation, Kyushu University, Fukuoka, Japan*

Received 18 June 2004; received in revised form 3 October 2004; accepted 22 October 2004

Available online 10 December 2004

Abstract

gp130-dependent signaling is known to play a critical role in the onset of heart failure. In that regard, cardiotrophin-1 (CT-1) activates several signaling pathways via gp130, and induces hypertrophy in neonatal rat cardiomyocytes. Among the mediators activated by CT-1, STAT3 is thought to be important for induction of cell hypertrophy, though its precise function in the CT-1 signaling pathway is not fully understood. In the present study, therefore, to better understand the significance of STAT3 activity in CT-1 signaling, we infected cultured cardiomyocytes with adenoviral vectors harboring a dominant-negative STAT3 mutant or one of two endogenous negative regulators of cytokine signaling via the Janus kinase (JAK)-signal transducer and activator of transcription (STAT) pathways [suppressor of cytokine signaling (SOCS) 1 and 3] and then examined their effects on three indexes of CT-1-induced cell hypertrophy: protein synthesis, secretion of brain natriuretic peptide and changes in cell surface area. In control cells, CT-1-induced both STAT3 phosphorylation and cell hypertrophy. Overexpression of dominant-negative STAT3 mutant suppressed CT-1-induced STAT3 phosphorylation, but did not affect cell hypertrophy. On the other hand overexpression of SOCS1 or SOCS3 inhibited both CT-1-induced STAT3 phosphorylation and cell hypertrophy. CT-1 also induced phosphorylations of ERK1/2 and ERK5 in cardiomyocytes, and those, too, were suppressed by overexpression of SOCSs. CT-1-induced cell hypertrophy was suppressed by overexpression of a dominant-negative MEK5 mutant, and not by overexpression of a dominant-negative MEK1 mutant. These findings indicate that the major pathway responsible for the hypertrophic responses to CT-1 is not JAK-STAT3 pathway nor MEK1-ERK1/2 pathway, but MEK5-ERK5 pathway.

Keywords: Cardiotrophin-1; Cytokine; ERK1/2; ERK5; STAT3; Cell signaling; Hypertrophy; Cardiomyocyte

1. Introduction

Cardiotrophin-1 (CT-1) is an interleukin-6 (IL-6)-related cytokine that exerts various hypertrophic and antiapoptotic effects via the gp130-leukemia inhibitory factor (LIF) receptor complex by activating several intracellular signaling in cardiomyocytes, including the Janus kinase (JAK)-signal transducer and activator of transcription (STAT) and mitogen-activated protein kinase (MAPK) pathways [1]. The receptors for IL-6-related cytokines share gp130 as a signal-transducing receptor component [1]. Its continuous activation in heart due, for example, to overexpression of IL-6 and its receptor is known to cause myocardial hypertrophy [2]. Conversely, ventricular restricted gp130-deficient mice display massive apoptosis of cardiomyocytes and are unable to achieve compensatory hypertrophy during aortic pressure overload [3]. So it is very important to elucidate the physi-

Abbreviations: BNP, brain natriuretic peptide; CT-1, cardiotrophin-1; ERK, extracellular signal-regulated kinase; ET-1, endothelin-1; GPCR, G-protein-coupled receptor; IL-6, interleukin-6; JAK, Janus kinase; LIF, leukemia inhibitory factor; MAPK, mitogen-activated protein kinase; MEK, MAPK/ERK kinase; PI3K, phosphatidylinositol 3-OH kinase; SOCS, suppressor of cytokine signaling; STAT, signal transducer and activator of transcription.

* Corresponding author. Tel.: +81-744-29-8850; fax: +81-744-22-9726.
E-mail address: yssaito@nmu-gw.naramed-u.ac.jp (Y. Saito).

0022-2828/$ - see front matter © 2004 Elsevier Ltd. All rights reserved.
doi:10.1016/j.yjmcc.2004.10.016

ological or pathophysiological role of IL-6-related cytokines in the heart.

On the other hand, little is known about the significance of the signaling pathways downstream of gp130 that mediates the phenotypic, namely hypertrophic and antiapoptotic effects of IL-6-related cytokines such as CT-1. We previously showed that CT-1 induces its antiapoptotic effects via the phosphatidylinositol 3-OH kinase (PI3K)-Akt pathway [4]. In addition, others have shown that LIF, which shares a receptor with CT-1, induces hypertrophy in cardiomyocytes via STAT3 [5], and that cardiac-specific overexpression of STAT3 leads to myocardial hypertrophy [6]. In those cases, however, the contribution made by STAT3 did not appear especially pronounced, making it unclear whether STAT3 mediated transduction in the principal pathway leading to hypertrophy. In that regard, we have shown that CT-1-induced STAT3 activation leads to upregulation of two endogenous negative regulators of cytokine signaling via JAK-STAT pathways [suppressor of cytokine signaling (SOCS) 1 and 3, also referred to as JAK-binding protein (JAB) and cytokine-inducible SH2 protein (CIS) 3/STAT-induced STAT inhibitor (SSI) 1 and 3] [7–9] in the heart [10].

Finally, Kodama et al. [11] have shown that the MAPK/extracellular signal-regulated kinase (ERK) kinase (MEK)1/2-ERK1/2 pathway is critically involved in LIF-induced cardiomyocyte hypertrophy. Moreover, Nicol et al. [12] recently reported that in cardiomyocytes LIF activates ERK5, a novel member of the MAPK family, and that a dominant-negative form of MEK5, the MAPK kinase directly responsible for activation of ERK5, inhibits LIF-induced elongation of cardiomyocytes.

With those as background, we hypothesized that the major molecule responsible for the hypertrophic responses to IL-6-related cytokines may not be STAT3, but ERK1/2 or ERK5. So in this study, we examined the effects of overexpressing SOCSs, dominant-negative mutant of STAT3, MEK1 or MEK5 on CT-1-induced cardiomyocyte hypertrophy with the aim of better understanding the significance of the STAT3 and MEK-ERK pathways in CT-1-induced cardiac hypertrophy.

2. Materials and methods

2.1. Materials

Recombinant rat CT-1 was prepared using a GST-fusion system (Pharmacia Biotechnology, Inc.) according to the manufacturer's instructions. Human endothelin-1 (ET-1) was purchased from Peptide Institute. Anti-STAT3, anti-phospho-STAT3 (Tyr705), anti-p44/42 MAPK (ERK1/2), anti-phospho-ERK1/2 (Thr202/Tyr204) and anti-phospho-ERK5 (Thr218/Tyr220) antibodies were from Cell Signaling Technology. Anti-ERK5/BMK1 antibody was from Upstate Biotechnology. Anti-SOCS3/CIS3 antibody was from Immuno-Biological Laboratories. PD98059 was from Calbiochem.

2.2. Recombinant adenoviruses

Adenoviral vectors harboring the genes for LacZ (Ad-LacZ), myc-tagged SOCS1 (AdSOCS1), myc-tagged SOCS3 (AdSOCS3), an HA-tagged dominant-negative STAT3 mutant (AdSTAT3F) in which phosphorylation-site Tyr705 was substituted with Phe [13], and Cre recombinase (AdCre) were gifts from Dr. Yasushi Hanakawa, Ehime University School of Medicine, Ehime, Japan [14]; an adenoviral vector containing the gene for a dominant-negative MEK5 mutant (AdMEK5KM) in which ATP-binding Lys106 was substituted with Met [15] was a gift from Dr. Eric N. Olson, University of Texas, Dallas, USA [12]; and an adenoviral vector harboring the gene for a dominant-negative MEK1 mutant (AdMEK1DN) in which Asp208 in the kinase subdomain VII was substituted with an Ala [16] was a gift from Dr. Seinosuke Kawashima, Kobe University, Kobe, Japan. Because of the toxic effect of SOCS1 on 293 cells used for recombinant virus production, a Cre-LoxP conditional expression system was employed to generate AdSOCS1 using the protocol described by Kanegae et al. [17]. For that reason, only AdSOCS1 was co-infected with AdCre. All adenoviral vectors harbor the cytomegalovirus enhancer and the chicken β-actin promoter.

2.3. Cardiomyocyte culture and adenovirus infection

Ventricular myocytes were prepared from 1-day-old Wistar rats using a Percoll gradient as previously described [18]. The investigation conforms to the Guiding Principles in the Care and Use of Animals (American Physiological Society). After collecting the myocytes from the gradient, they were preplated on noncoated dishes for 1 h, after which the unattached cells were collected; this cell population consisted of >97% myocytes as assessed by immunofluorescence with anti-rat sarcomeric actin antibody (DAKO Japan Co., Ltd.). The myocytes were then plated on gelatin-coated dishes in serum-containing medium for 24 h. The medium was then replaced with serum-free medium, and the cells were infected for 24 h with one of the recombinant adenoviruses at a multiplicity of infection (MOI) of 10 viral particles per cell. Under these conditions, >99% of the myocytes were infected (assessed by X-gal staining or immunocytochemistry with anti-tag antibodies). Thereafter, the cells were treated with 10^{-9} mol/l CT-1 or 10^{-8} mol/l ET-1 for the indicated times. In some cases, the MEK inhibitor PD98059 was applied for 30 min prior to addition of CT-1 or ET-1.

2.4. Western blot analysis

After incubating the cells with CT-1 or ET-1 for the indicated times, they were washed with ice-cold phosphate-buffered saline (PBS) and lyzed with lysis buffer (Cell Signaling Technology). The resultant whole-cell protein extracts were subjected to 10% SDS-PAGE, and the resolved proteins were electrophoretically transferred onto polyvinylidene dif-

luoride membranes (Bio-Rad Laboratories). The membranes were then blocked with 5% skim milk (Difco Laboratories) and probed with the indicated antibodies.

2.5. Analysis of protein synthesis in cultured cells

Protein synthesis in cultured cardiomyocytes was evaluated using [^{3}H]-leucine incorporation as an index. Following incubation with CT-1 or ET-1, the cells were cultured for 24 h, after which 3 μCi of [^{3}H]-leucine (Amersham Life Science) was added for an additional 24 h. After washing twice with ice-cold PBS, the cells were incubated in 10% trichloroacetic acid for 30 min at 4 °C. The resultant precipitate was solubilized in 0.2 N NaOH for >4 h, and the radioactivity was measured in a liquid scintillation counter.

2.6. Radioimmunoassay for brain natriuretic peptide

Levels of brain natriuretic peptide (BNP) in medium conditioned for 48 h by cardiomyocytes after stimulation with CT-1 or ET-1 was measured using a specific radioimmunoassay as previously described [19].

2.7. Statistical analysis

Data are presented as mean ± standard deviations (S.D.) of results of four independent experiments. Unpaired Student's *t*-tests were used to determine significant differences between two groups, and ANOVA with post hoc Fisher's tests was used to determine significant differences among three or four groups. Values of $P < 0.05$ were considered significant.

3. Results

3.1. Effects of SOCSs and STAT3F on CT-1-induced STAT3 phosphorylation

First, to determine whether SOCSs are the true endogenous negative regulators of CT-1 signaling in our cultured cardiomyocytes, Western blot analysis was carried out using samples from CT-1-treated cardiomyocytes probed with anti-SOCS3 antibody. As shown in Fig. 1A, upregulation of SOCS3 protein was confirmed in CT-1-treated cardiomyocytes. We previously showed that CT-1 induced tyrosine phosphorylation of STAT3 in cardiomyocytes, and that the response peaked within 5–15 min of CT-1 application [20]. Next, therefore, we examined the effects of overexpressing SOCS1, SOCS3 and STAT3F on levels of STAT3 tyrosine phosphorylation after 10 min of CT-1 stimulation. AdSOCS1, AdSOCS3 and AdSTAT3F did not have an influence on the basal phosphorylation of STAT3 (Fig. 1B). As shown in Figs. 1B, and 1C, CT-1 induced substantial phosphorylation of STAT3 in cardiomyocytes infected with AdLacZ. This effect was completely blocked in cardiomyocytes infected with AdSOCS1 or AdSOCS3, and significantly inhibited in

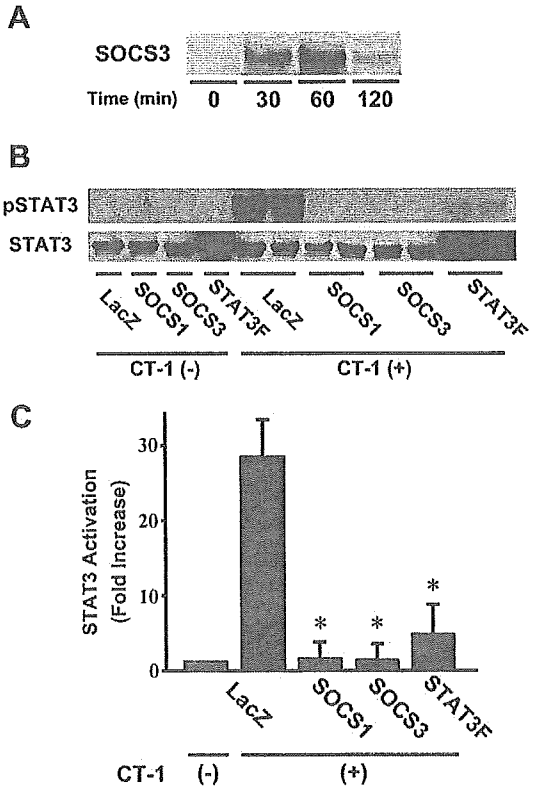

Fig. 1. SOCS3 expression induced by CT-1 and effects of SOCS1, SOCS3 and STAT3F on CT-1-induced phosphorylation of STAT3. (**A**) Representative Western blots showing the time course SOCS3 protein expression in CT-1-treated cardiomyocytes without adenovirus infection. (**B**) Representative Western blots showing the effects of SOCS1, SOCS3 and STAT3F on CT-1-induced phosphorylation of STAT3. Cardiomyocytes infected with AdLacZ, AdSOCS1, AdSOCS3 or AdSTAT3F were treated with 10^{-9} mol/L CT-1 for 10 minutes, after which cell lysates were harvested. (**C**) Phospho-STAT3 (pSTAT3) and STAT3 were measured densitometrically from immunoblots like those in panel B. The ratio of pSTAT3 to STAT3 was normalized to that in AdLacZ-infected cardiomyocytes without CT-1 treatment, which was assigned a value of 1. Only in regard to AdSTAT3F-infected group, the ratio to the average STAT3 of the other adenovirus-infected groups was used. Values are means ± S.D. (n = 8) of four independent experiments, each experiment performed with two distinct samples; $^*P < 0.01$ vs. LacZ with CT-1.

cardiomyocytes infected with AdSTAT3F. The apparently augmented expression of STAT3 in cardiomyocytes infected with AdSTAT3F reflects the cross-reaction of anti-STAT3 antibody with overexpressed STAT3F, and is indicative of the efficiency of the protein expression in cardiomyocytes transfected using these recombinant adenoviral vectors.

3.2. Effects of SOCSs and STAT3F on CT-1-induced cardiomyocyte hypertrophy

We next examined the effects of overexpressing SOCS1, SOCS3 or STAT3F on CT-1-induced hypertrophy of cardiomyocytes. For comparison, ET-1, a G-protein-coupled receptor (GPCR) agonist, was also used to induce a distinct form of cardiomyocyte hypertrophy [21]. We first evaluated CT-1- and ET-1-induced [^{3}H]-leucine incorporation as an index of protein synthesis. As shown in Fig. 2A, CT-1 significantly increased [^{3}H]-leucine incorporation in cardiomyocytes

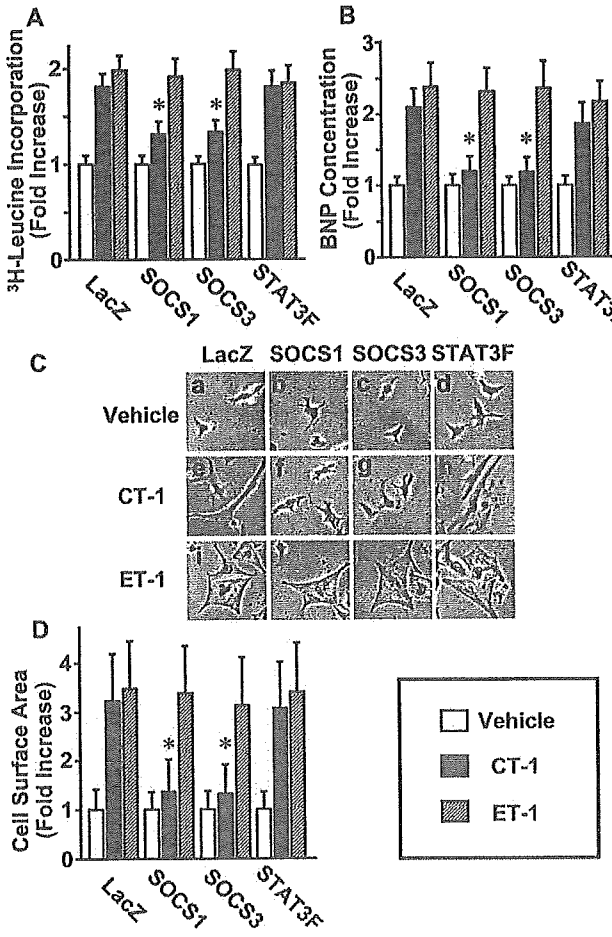

Fig. 2. Effects of SOCS1, SOCS3 and STAT3F on CT-1-induced cardiomyocyte hypertrophy. Cardiomyocytes infected with AdLacZ, AdSOCS1, AdSOCS3 or AdSTAT3F were treated with vehicle (open bars), 10^{-9} mol/L CT-1 (solid bars) or 10^{-8} mol/L ET-1 (hatched bars). The fold increase is relative to vehicle-treated cells of each adenovirus-infected group. **(A)** ^{3}H-leucine incorporation by cardiomyocytes during the period from 24 to 48 hours after treatment. **(B)** BNP concentration in the cultured media 48 hours after treatment. **(C)** Phase-contrast photographs of cultured cardiomyocytes taken 48 hours after treatment with vehicle *(a-d)*, CT-1 *(e-h)* or ET-1 *(i-l)*. **(D)** Cell surface areas were analyzed using NIH Image software. A total of 100 cells were examined for each group. The experiments were repeated four times independently, and each was performed with six distinct samples (**A, B**). Values are means ± S.D. (n = 24 in A and B, n = 100 in D); $^*P < 0.05$ vs. LacZ with CT-1.

infected with AdLacZ. This effect was significantly inhibited by infection with AdSOCS1 or AdSOCS3 but, somewhat surprisingly, not by infection with AdSTAT3F. Infection with AdSOCS1, AdSOCS3 or AdSTAT3F had no effect on ET-1-induced [^{3}H]-leucine incorporation.

The effects of AdSOCS1, AdSOCS3 and AdSTAT3F on BNP secretion from cardiomyocytes paralleled their effects on [^{3}H]-leucine incorporation (Fig. 2B)—i.e. infection with AdSOCS1 or AdSOCS3 significantly inhibited CT-1-induced BNP secretion, whereas infection with AdSTAT3F did not. ET-1-induced BNP secretion was unaffected by AdSOCS1, AdSOCS3 or AdSTAT3F.

CT-1- and ET-1-induced cardiomyocyte hypertrophy was also examined by evaluating their effect on cell shape and surface area. Consistent with an earlier report [21], CT-1 induced a characteristic hypertrophy in cardiomyocytes infected with AdLacZ (Fig. 2Ce)—i.e. it elicited pronounced increases in cell length, but did not significantly affect the width. ET-1, by contrast, elicited increases in both cell length and width (Fig. 2Ci). Infection with AdSOCS1 or AdSOCS3 (Fig. 2Cf, g and 2D), but not AdSTAT3F (Fig. 2Ch and 2D), inhibited CT-1-induced changes in cell shape and size. ET-1-induced changes in cell shape and size were unaffected by AdSOCS1, AdSOCS3 or AdSTAT3F (Fig. 2Cj-l and 2D).

3.3. Effects of SOCSs and STAT3F on CT-1-induced ERK phosphorylation

Collectively, the results presented so far indicate that inhibition of STAT3 alone does not inhibit CT-1-induced cardiomyocyte hypertrophy. Only when SOCSs are used to inhibit other signaling pathways is the hypertrophy inhibited. In that regard, CT-1 is known to also induce activation of ERK1/2 in cardiomyocytes [1], while LIF, another IL-6-related cytokine, has been reported to induce activation of ERK5 in cardiomyocytes [12]. With that in mind, we examined the effects of overexpressing SOCS1, SOCS3 or STAT3F on CT-1-induced activation (phosphorylation) of ERK1/2 and ERK5. AdSOCS1, AdSOCS3 and AdSTAT3F did not affect the basal phosphorylation of ERK1/2 nor ERK5 (Fig. 3D). We found that CT-1-induced phosphorylation of both ERK1/2 and ERK5 that peaked within ~10 min (Fig. 3A–C), and these effects were significantly inhibited by infection with AdSOCS1 or AdSOCS3, but not AdSTAT3F (Fig. 3D–F). Thus, the effects of overexpressing SOCS1, SOCS3 or STAT3F on CT-1-induced ERK activation differed from the effects on STAT3 activation, but paralleled the effects on cardiomyocyte hypertrophy.

3.4. Effects of PD98059 on CT-1-induced ERK phosphorylation and on CT-1-induced cardiomyocyte hypertrophy

The MEK1 inhibitor PD98059 [22] was recently shown to also inhibit MEK5, the specific upstream activator of ERK5, though at a somewhat higher concentration [23]. Likewise, we found that PD98059 concentration-dependently inhibited CT-1-induced phosphorylation of both ERK1/2 and ERK5, but that it was a more potent inhibitor of the former (Fig. 4A–C). PD98059 also inhibited both CT-1- and ET-1-induced [^{3}H]-leucine incorporation and BNP secretion (Fig. 4D, E). It is noteworthy that the potency of the inhibitory effect of PD98059 on the activities of CT-1 and ET-1 paralleled the potency of its effect on the phosphorylation of ERK5 and ERK1/2, respectively.

3.5. Effects of dominant-negative MEK1 and MEK5 mutants on CT-1-induced cardiomyocyte hypertrophy

The results obtained with PD98059 were confirmed when we examined the effects of overexpressing dominant-negative

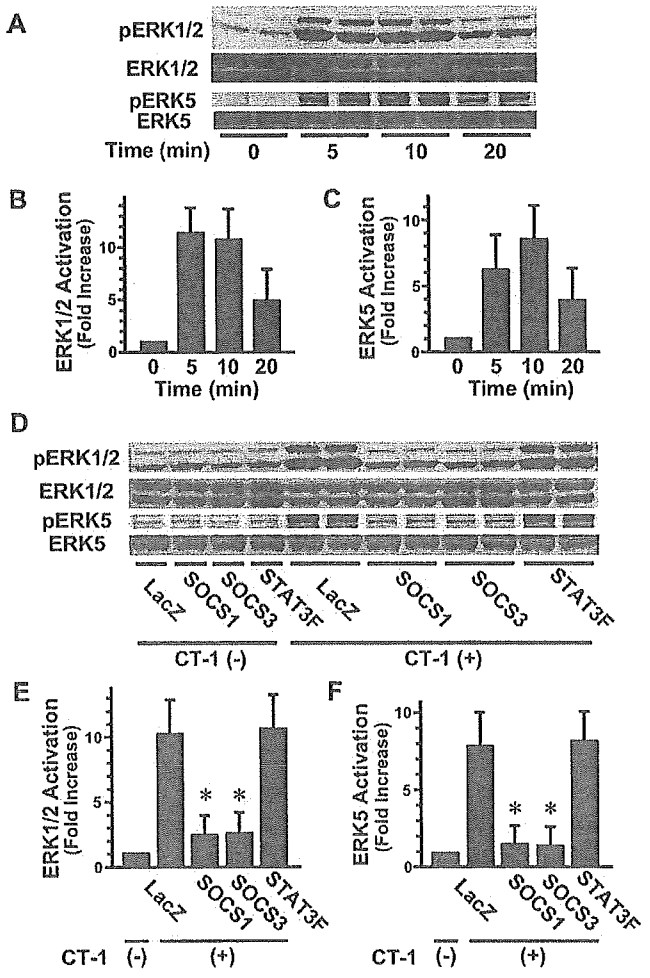

Fig. 3. Time course of CT-1-induced phosphorylation of ERK1/2 and ERK5, and effects of SOCS1, SOCS3 and STAT3F on CT-1-induced phosphorylation of ERK1/2 and ERK5. (A) Representative Western blots showing the time course of CT-1-induced phosphorylation of ERK1/2 and ERK5. Cardiomyocytes infected with AdLacZ were stimulated with 10^{-9} mol/L CT-1 for the indicated times, after which cell lysates were harvested. (B) Phospho-ERK1/2 (pERK1/2) and ERK1/2 were measured densitometrically from immunoblots like those in panel A. The ratio of pERK1/2 to ERK1/2 was normalized to that in cardiomyocytes without CT-1 treatment, which was assigned a value of 1. (C) Phospho-ERK5 (pERK5) and ERK5 were analyzed as panel B. (D) Representative Western blots showing the effects of SOCS1, SOCS3 and STAT3F on CT-1-induced phosphorylation of ERK1/2 and ERK5. Cardiomyocytes infected with AdLacZ, AdSOCS1, AdSOCS3 or AdSTAT3F were treated with 10^{-9} mol/L CT-1 for 10 min, after which the cell lysates were harvested. (E) Phospho-ERK1/2 (pERK1/2) and ERK1/2 were measured densitometrically from immunoblots like those in panel D. The ratio of pERK1/2 to ERK1/2 was normalized to that in AdLacZ-infected cardiomyocytes without CT-1 treatment, which as assigned a value of 1. (F) Phospho-ERK5 (pERK5) and ERK5 were analyzed in the same way as panel E. Values are means ± S.D. (n = 8) of four independent experiments, each experiment performed with two distinct samples; $^*P < 0.05$ vs. LacZ with CT-1.

MEK1 or MEK5 mutants on CT-1-induced phosphorylation of ERKs and cardiomyocyte hypertrophy. As shown in Fig. 5, infection with AdMEK1DN inhibited both the basal phosphorylation of ERK1/2 and CT-1-induced phosphorylation of ERK1/2, but did not have an influence on the phosphorylation of ERK5. On the other hand, infection with AdMEK5KM inhibited both the basal phosphorylation of

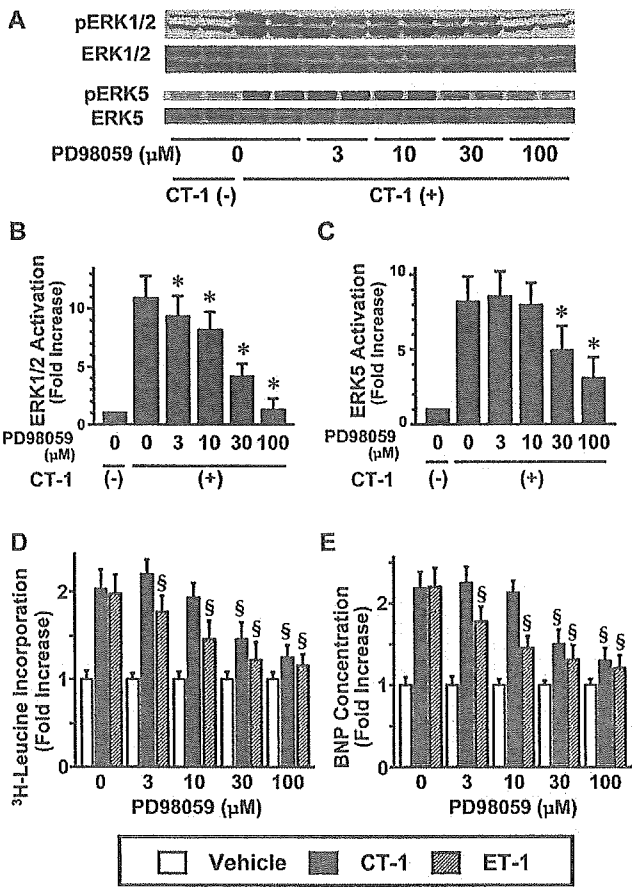

Fig. 4. Effects of PD98059 on CT-1-induced phosphorylation of ERK1/2 and ERK5 and CT-1- and ET-1-induced cardiomyocyte hypertrophy. Cardiomyocytes cultured with the indicated concentration of PD98059 were treated with vehicle (open bars), 10^{-9} mol/L CT-1 (solid bars) or 10^{-8} mol/L ET-1 (hatched bars). (A) Representative Western blots of phospho-ERK1/2 (pERK1/2) and phospho-ERK5 (pERK5) in lysates harvested after 10 minutes of CT-1 treatment. (B) pERK1/2 and ERK1/2 were measured densitometrically from immunoblots like those in panel A. The ratio of pERK1/2 to ERK1/2 was normalized to that in cardiomyocytes without CT-1 treatment, which as assigned a value of 1. (C) pERK5 and ERK5 were analyzed in the same way as panel B. (D) ^{3}H-leucine incorporation by cardiomyocytes during the period from 24 to 48 hours after treatment. (E) BNP concentration in the cultured media 48 hours after treatment. Fold increase is relative to vehicle-treated cells in each concentration group. The experiments were repeated four times independently, and each was performed with two distinct samples (A-C) or with sis distinct samples (D, E). Values are means ± S.D. (n = 8 in A to C, n = 24 in D and E); $^*P < 0.05$ vs. PD98059 (-) with CT-1, §$P < 0.05$ vs. LacZ with CT-1 or ET-1, correspondently.

ERK5 and CT-1-induced phosphorylation of ERK5, but did not have an influence on the phosphorylation of ERK1/2. And as shown in Fig. 6, infection with AdMEK5KM but not AdMEK1DN significantly inhibited CT-1-induced increases in [^{3}H]-leucine incorporation, BNP secretion and cell surface area. Conversely, infection with AdMEK1DN but not AdMEK5KM inhibited the ET-1-induced effects.

4. Discussion

The aim of the present study was to assess the significance of the STAT3 and MEK-ERK pathways in CT-1-induced

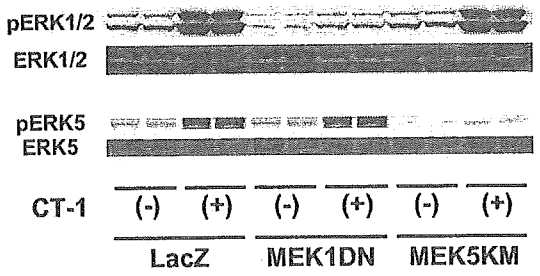

Fig. 5. Effects of dominant-negative MEK1 (MEK1DN) and MEK5 (MEK5KM) mutants on CT-1-induced phosphorylation of ERK1/2 and ERK5. Representative Western blots of phospho-ERK1/2 (pERK1/2) and phospho-ERK5 (pERK5) in lysates harvested after 10 minutes of CT-1 treatment.

hypertrophy of cultured neonatal rat ventricular myocytes. Among several pathways activated by IL-6-related cytokines in cardiomyocytes, the STAT3 pathway is reportedly important for mediating cardiomyocyte hypertrophy [5,6,24]. In our study, however, a dominant-negative STAT3 mutant did not inhibit CT-1-induced cardiomyocyte hypertrophy, although it suppressed activation (phosphorylation) of STAT3. We can not explain strictly the discrepancy of our results from previous study [5], but we think that it may be attributable to the difference of culture conditions, for example the degree of fibroblasts contamination. We have confirmed the existence of STAT3 in cardiac fibroblasts and its phosphorylation induced by CT-1 (data not shown). With the results in our study, the major pathway leading from CT-1 binding to the gp130 complex to cardiomyocyte hypertrophy is not via STAT3. On the other hand, two recently identified [7–9] endogenous negative regulators of cytokine signaling via JAK-STAT pathways, SOCS1 and SOCS3, significantly inhibited both STAT3 phosphorylation and the hypertrophic effects of CT-1, which is consistent with an earlier report [14]. In addition, SOCS1/3 and dominant-negative STAT3 mutant had the same influence on the hypertrophic effects of LIF, another member of IL-6-related cytokines (data not shown), indicating that these differential effects of SOCSs vs. dominant-negative STAT3 are not CT-1 specific, but shared with other members of IL-6-related cytokines. The key question then was what gp130-dependent signaling pathway do SOCSs suppress to inhibit CT-1-induced hypertrophy?

Among the possibilities are the STAT1 pathway [25], the PI3K-Akt pathway [26] and the MEK1/2-ERK1/2 pathway [11,16], all of which appear to be involved in LIF-induced cardiomyocyte hypertrophy. The first two are easily ruled out. We found that dominant-negative STAT3 inhibited CT-1-induced phosphorylation of not only STAT3 but also STAT1 (data not shown), most likely because STAT3 and STAT1 share docking sites for JAK1/2 [1]. Therefore, if CT-1 acted via STAT1, we would expect its effects to have been inhibited by the dominant-negative STAT3 mutant. As for the PI3K-Akt pathway, we previously showed that this pathway is largely responsible for CT-1's antiapoptotic effects rather than cell hypertrophy [4].

This leaves the MEK-ERK pathways. PD98059 is known as a specific inhibitor of MEK1 [22], but some reports suggest that it also inhibits MEK5 at a somewhat higher concentration [23,27]. Consistent with those results, we found that at concentrations <30 μM PD98059 selectively inhibits evoked ERK1/2 phosphorylation and ET-1-induced cardiomyocyte hypertrophy. At concentrations ≥30 μM, however, PD98059 also inhibits ERK5 phosphorylation and CT-1-induced cardiomyocyte hypertrophy. On the other hand, it is also known that PD98059 loses specificity at the higher concentrations. So we added the examinations with dominant-negative MEK1 or MEK5 mutant to confirm our hypothesis acquired from the examinations with PD98059. Dominant-negative MEK1 mutant partially inhibited ET-1-induced hypertrophy, but had not effect on CT-1-induced hypertro-

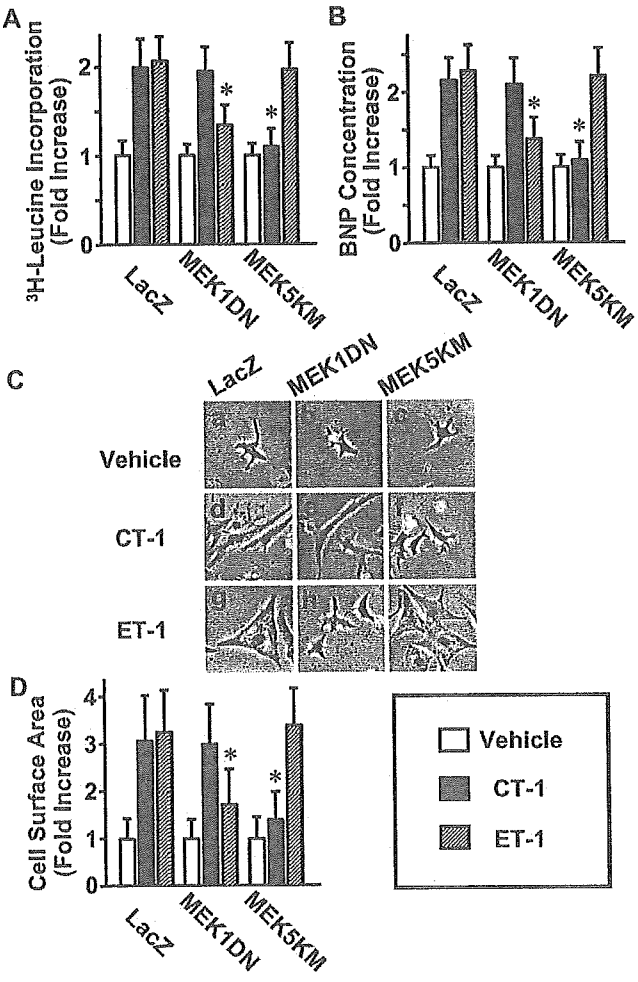

Fig. 6. Effects of dominant-negative MEK1 (MEK1DN) and MEK5 (MEK5KM) mutants on CT-1-induced cardiomyocyte hypertrophy. Cardiomyocytes infected with AdLacZ, AdMEK1DN or AdMEK5KM were treated with vehicle (open bars), 10^{-9} mol/L CT-1 (solid bars) or 10^{-8} mol/L ET-1 (hatched bars). The fold increase is relative to vehicle-treated cells in each adenovirus-infected group. **(A)** ^{3}H-leucine incorporation by cardiomyocytes during the period from 24 to 48 hours after treatment. **(B)** BNP concentration in the cultured media 48 hours after treatment. **(C)** Phase-contrast photographs of cultured cardiomyocytes obtained 48 hours after treatment with vehicle *(a-c)*, CT-1 *(d-f)* or ET-1 *(g-i)*. **(D)** Cell surface areas were analyzed using NIH Image software. A total of 100 cells were examined for each group. The experiments were repeated four times independently, and each was performed with six distinct samples **(A, B)**. Values are means ± S.D. (n = 24 in A and B, n = 100 in D); $^*P < 0.05$ vs. LacZ with CT-1.

phy, whereas dominant-negative MEK5 mutant almost completely inhibited CT-1-induced hypertrophy, but had no effect on ET-1-induced hypertrophy. We therefore conclude that CT-1-induced cardiomyocyte hypertrophy is mediated mainly via a MEK5-ERK5 pathway, while ET-1-induced hypertrophy is at least partially via a MEK1/2-ERK1/2 pathway. The fact that SOCSs inhibited CT-1-induced phosphorylation of ERK5 indicates they suppress hypertrophic responses to CT-1 through inhibition of a MEK5-ERK5 pathway. These conclusions are further supported by the findings that gp130-deficient [28] and ERK5-deficient mice [29] show similar embryonic cardiovascular defects, suggesting ERK5 is an important mediator situated downstream of gp130 during cardiovascular development.

CT-1-induced cardiomyocyte hypertrophy is distinct from that induced by GPCR agonists including ET-1 and angiotensin II [21]. Pathophysiological significance of GPCR agonists in the heart is undoubted because of the clinical usefulness of angiotensin-converting-enzyme (ACE) inhibitors [30–33]. On the other hand, there is little clinical evidence concerning IL-6-related cytokines including CT-1. With regard to mouse models, however, IL-6-related cytokines are known to induce concentric hypertrophy via gp130 in in vivo heart [2]. Although here we have shown the significance of the MEK5-ERK5 pathway in cardiomyocyte hypertrophy induced by CT-1, a member of IL-6-related cytokines, activated MEK5 has been shown to induce eccentric, not concentric, hypertrophy in in vivo heart [12]. That is to say, activation of only a MEK5-ERK5 pathway can not account for the cardiac phenotype induced by IL-6-related cytokines. Several signaling pathways including JAK-STATs, MEK-ERKs and PI3K-Akt pathways probably cooperate and express the cardiac phenotype induced by IL-6-related cytokines. So it is necessary to investigate more detailed role of not only a MEK5-ERK5 pathway, but also the other signaling pathways downstream of gp130 in the cardiomyocyte or in the heart stimulated with IL-6-related cytokines. Furthermore, it is expected to elucidate the clinical significance of IL-6-related cytokines in the heart.

Finally, our finding that the MEK5-ERK5 pathway plays a critical role in CT-1-induced cardiomyocyte hypertrophy raises the question, what is the role of STAT3 in cardiomyocytes? Kunisada et al. [6] reported that STAT3 transduces a protective signal against doxorubicin-induced cardiomyopathy, but we detected no related phenotypes in cardiomyocytes overexpressing a dominant-negative STAT3 mutant. It may be that the key role played by STAT3 in cardiomyocytes involves the induction of SOCSs [10] and subsequent inhibition of the MEK5-ERK5 pathway.

Acknowledgments

This work was supported in part by research grants from the Japanese Ministry of Education, Culture, Sports, Science and Technology, the Japanese Ministry of Health, Labor and Welfare, and the Research for the Future Program of the Japan Society for the Promotion of Science (JSPS-RFTF96I00204 and 98L00801), and by grants from the Japanese Cardiovascular Research Foundation, Uehara Memorial Foundation and the Smoking Research Foundation. We thank Dr. E. Olson, Dr. S. Kawashima and Dr. Y. Hanakawa for providing adenovirus vectors and thanks to K. Okamura for her excellent secretarial work.

References

[1] Wollert KC, Chien KR. Cardiotrophin-1 and the role of gp130-dependent signaling pathways in cardiac growth and development. J Mol Med 1997;75:492–501.

[2] Hirota H, Yoshida K, Kishimoto T, Taga T. Continuous activation of gp130, a signal-transducing receptor component for interleukin 6-related cytokines, causes myocardial hypertrophy in mice. Proc Natl Acad Sci USA 1995;92:4862–8.

[3] Hirota H, Chen J, Betz UA, Rajewsky K, Gu Y, Ross Jr. J, et al. Loss of a gp130 cardiac muscle cell survival pathway is a critical event in the onset of heart failure during biomechanical stress. Cell 1999;97:189–98.

[4] Kuwahara K, Saito Y, Kishimoto I, Miyamoto Y, Harada M, Ogawa E, et al. Cardiotrophin-1 phosphorylates akt and BAD, and prolongs cell survival via a PI3K-dependent pathway in cardiac myocytes. J Mol Cell Cardiol 2000;32:1385–94.

[5] Kunisada K, Tone E, Fujio Y, Matsui H, Yamauchi-Takihara K, Kishimoto T. Activation of gp130 transduces hypertrophic signals via STAT3 in cardiac myocytes. Circulation 1998;98:346–52.

[6] Kunisada K, Negoro S, Tone E, Funamoto M, Osugi T, Yamada S, et al. Signal transducer and activator of transcription 3 in the heart transduces not only a hypertrophic signal but a protective signal against doxorubicin-induced cardiomyopathy. Proc Natl Acad Sci USA 2000;97:315–9.

[7] Starr R, Willson TA, Viney EM, Murray LJ, Rayner JR, Jenkins BJ, et al. A family of cytokine-inducible inhibitors of signalling. Nature 1997;387:917–21.

[8] Endo TA, Masuhara M, Yokouchi M, Suzuki R, Sakamoto H, Mitsui K, et al. A new protein containing a SH2 domain that inhibits JAK kinases. Nature 1997;387:921–4.

[9] Naka T, Narazaki M, Hirata M, Matsumoto T, Minamoto S, Aono A, et al. Structure and function of a new STAT-induced STAT inhibitor. Nature 1997;387:924–9.

[10] Hamanaka I, Saito Y, Yasukawa H, Kishimoto I, Kuwahara K, Miyamoto Y, et al. Induction of JAB/SOCS-1/SSI-1 and CIS3/SOCS-3/SSI-3 is involved in gp130 resistance in cardiovascular system in rat treated with cardiotrophin-1 in vivo. Circ Res 2001;88:727–32.

[11] Kodama H, Fukuda K, Pan J, Sano M, Takahashi T, Kato T, et al. Significance of ERK cascade compared with JAK/STAT and PI3-K pathway in gp130-mediated cardiac hypertrophy. Am J Physiol Heart Circ Physiol 2000;279:H1635–H1644.

[12] Nicol RL, Frey N, Pearson G, Cobb M, Richardson J, Olson EN. Activated MEK5 induces serial assembly of sarcomeres and eccentric cardiac hypertrophy. EMBO J 2001;20:2757–67.

[13] Minami M, Inoue M, Wei S, Takeda K, Matsumoto M, Kishimoto T, et al. STAT3 activation is a critical step in gp130-mediated terminal differentiation and growth arrest of a myeloid cell line. Proc Natl Acad Sci USA 1996;93:3963–6.

[14] Yasukawa H, Hoshijima M, Gu Y, Nakamura T, Pradervand S, Hanada T, et al. Suppressor of cytokine signaling-3 is a biomechanical stress-inducible gene that suppresses gp130-mediated cardiac myocyte hypertrophy and survival pathways. J Clin Invest 2001;108:1459–67.

[15] English JM, Pearson G, Hockenberry T, Shivakumar L, White MA, Cobb MH. Contribution of the ERK5/MEK5 pathway to Ras/Raf signaling and growth control. J Biol Chem 1999;274:31588–92.

[16] Ueyama T, Kawashima S, Sakoda T, Rikitake Y, Ishida T, Kawai M, et al. Requirement of activation of the extracellular signal-regulated kinase cascade in myocardial cell hypertrophy. J Mol Cell Cardiol 2000;32:947–60.

[17] Kanegae Y, Lee G, Sato Y, Tanaka M, Nakai M, Sakaki T, et al. Efficient gene activation in mammalian cells by using recombinant adenovirus expressing site-specific Cre recombinase. Nucleic Acids Res 1995;23:3816–21.

[18] Harada M, Itoh H, Nakagawa O, Ogawa Y, Miyamoto Y, Kuwahara K, et al. Significance of ventricular myocytes and nonmyocytes interaction during cardiocyte hypertrophy: evidence for endothelin-1 as a paracrine hypertrophic factor from cardiac nonmyocytes. Circulation 1997;96:3737–44.

[19] Nakao K, Ogawa Y, Suga S, Imura H. Molecular biology and biochemistry of the natriuretic peptide system. I: natriuretic peptides. J Hypertens 1992;10:907–9012.

[20] Kuwahara K, Saito Y, Harada M, Ishikawa M, Ogawa E, Miyamoto Y, et al. Involvement of cardiotrophin-1 in cardiac myocyte–nonmyocyte interactions during hypertrophy of rat cardiac myocytes in vitro. Circulation 1999;100:1116–24.

[21] Wollert KC, Taga T, Saito M, Narazaki M, Kishimoto T, Glembotski CC, et al. Cardiotrophin-1 activates a distinct form of cardiac muscle cell hypertrophy. Assembly of sarcomeric units in series VIA gp130/leukemia inhibitory factor receptor-dependent pathways. J Biol Chem 1996;271:9535–45.

[22] Alessi DR, Cuenda A, Cohen P, Dudley DT, Saltiel AR. PD 098059 is a specific inhibitor of the activation of mitogen-activated protein kinase kinase in vitro and in vivo. J Biol Chem 1995;270:27489–94.

[23] Kamakura S, Moriguchi T, Nishida E. Activation of the protein kinase ERK5/BMK1 by receptor tyrosine kinases. Identification and characterization of a signaling pathway to the nucleus. J Biol Chem 1999; 274:26563–71.

[24] Railson JE, Liao Z, Brar BK, Buddle JC, Pennica D, Stephanou A, et al. Cardiotrophin-1 and urocortin cause protection by the same pathway and hypertrophy via distinct pathways in cardiac myocytes. Cytokine 2002;17:243–53.

[25] Kodama H, Fukuda K, Pan J, Makino S, Baba A, Hori S, et al. Leukemia inhibitory factor, a potent cardiac hypertrophic cytokine, activates the JAK/STAT pathway in rat cardiomyocytes. Circ Res 1997;81:656–63.

[26] Oh H, Fujio Y, Kunisada K, Hirota H, Matsui H, Kishimoto T, et al. Activation of phosphatidylinositol 3-kinase through glycoprotein 130 induces protein kinase B and p70 S6 kinase phosphorylation in cardiac myocytes. J Biol Chem 1998;273:9703–10.

[27] Mody N, Leitch J, Armstrong C, Dixon J, Cohen P. Effects of MAP kinase cascade inhibitors on the MKK5/ERK5 pathway. FEBS Lett 2001;502:21–4.

[28] Yoshida K, Taga T, Saito M, Suematsu S, Kumanogoh A, Tanaka T, et al. Targeted disruption of gp130, a common signal transducer for the interleukin 6 family of cytokines, leads to myocardial and hematological disorders. Proc Natl Acad Sci USA 1996;93:407–11.

[29] Regan CP, Li W, Boucher DM, Spatz S, Su MS, Kuida K. Erk5 null mice display multiple extraembryonic vascular and embryonic cardiovascular defects. Proc Natl Acad Sci USA 2002;99:9248–53.

[30] The CONSENSUS Trial Study Group. Effects of enalapril on mortality in severe congestive heart failure. Results of the Cooperative North Scandinavian Enalapril Survival Study (CONSENSUS). N Engl J Med 1987;316:1429–35.

[31] The SOLVD Investigators. Effect of enalapril on survival in patients with reduced left ventricular ejection fractions and congestive heart failure. N Engl J Med 1991;325:293–302.

[32] Swedberg K, Held P, Kjekshus J, Rasmussen K, Ryden L, Wedel H. Effects of the early administration of enalapril on mortality in patients with acute myocardial infarction. Results of the Cooperative New Scandinavian Enalapril Survival Study II (CONSENSUS II). N Engl J Med 1992;327:678–84.

[33] The SOLVD Investigators. Effect of enalapril on mortality and the development of heart failure in asymptomatic patients with reduced left ventricular ejection fractions. N Engl J Med 1992;327:685–91.

Osteoporos Int (2005) 16: 907–913
DOI 10.1007/s00198-004-1786-z

ORIGINAL ARTICLE

Decreased bone mineral density at the distal radius, but not at the lumbar spine or the femoral neck, in Japanese type 2 diabetic patients

T. Majima · Y. Komatsu · T. Yamada · Y. Koike
M. Shigemoto · C. Takagi · I. Hatanaka · K. Nakao

Received: 1 June 2004 / Accepted: 18 August 2004 / Published online: 19 November 2004

Abstract The purpose of this study is to assess the association between type 2 diabetes and bone mineral density. This study included 145 Japanese patients (64 men and 81 women) with type 2 diabetes and 95 non-diabetic control subjects (41 men and 54 women) of similar age. We measured bone mineral density (BMD) at the sites with different cortical/cancellous bone ratio (lumbar spine, femoral neck, and distal radius) using dual-energy X-ray absorptiometry. BMD and Z score at the distal radius were significantly lower in type 2 diabetic patients than those in control subjects, and in type 2 diabetic patients, the Z score at the distal radius was lower than that at their own lumbar spine and femoral neck. In type 2 diabetic patients, negative correlation between BMD and the mean HbA1c during the previous 2 years was found significantly at the distal radius in both genders and at the femoral neck in women. These results indicate the selective cortical bone loss in type 2 diabetes and suggest the importance of also determining BMD at the radius and keeping good metabolic control to prevent bone loss in type 2 diabetic patients.

Keywords Bone mineral density · Distal radius · Insulin levels · Type 2 diabetes mellitus

T. Majima · T. Yamada · Y. Koike · M. Shigemoto
C. Takagi · I. Hatanaka
Department of Endocrinology and Metabolism,
Rakuwakai Otowa Hospital, Kyoto, Japan

Y. Komatsu (✉) · K. Nakao
Department of Medicine and Clinical Science,
Kyoto University Graduate School of Medicine,
54 Shogoin Kawahara-cho Sakyo-ku,
606-8507 Kyoto, Japan
E-mail: komatsuy@barium.rirc.kyoto-u.ac.jp
Tel.: +81-75-7513168
Fax: +81-75-7719452

Introduction

Decreased bone mineral density (BMD) is an established complication of type 1 diabetes [1, 2]. However, contradictory results have been reported in BMD of type 2 diabetic patients thus far: several studies have shown that BMDs at the lumbar spine and the femoral neck were either unaltered [2, 3, 4, 5, 6, 7, 8, 9, 10] or increased [3, 6, 7, 8, 10, 11, 12, 13], rarely decreased [4, 10, 14] and that BMD at the distal radius was decreased [1, 15], not different [3, 6], or increased [3]. These complicated results suggest that examining BMDs at different sites may reveal different results, especially in type 2 diabetic patients. Therefore, it seems insufficient to measure the BMD of type 2 diabetic patients at a single site. Thus, in this study, we measured the BMD of Japanese type 2 diabetic men and women at the sites with different cortical/cancellous bone ratio: lumbar spine, femoral neck, and distal radius, using dual-energy X-ray absorptiometry (DXA).

Some papers reported that BMD was decreased more severely in the poorly controlled type 2 diabetic patients [1, 14]. On the other hand, some papers reported that insulin was an important factor in maintaining BMD [16, 17, 18, 19]. Japanese type 2 diabetic patients have the racial feature that they are mildly obese, with decreased capacity of insulin secretion, from a relatively early stage of the disease [20, 21]. It is, therefore, of interest to assess the relationship of BMD with BMI, the metabolic control and the capacity of insulin secretion in Japanese type 2 diabetic patients.

Subjects and methods

Subjects

One hundred and forty-five Japanese patients with type 2 diabetes (64 men and 81 women) were included in this study (Table 1). They were randomly selected from patients attending the diabetes clinic of Rakuwakai Ot-

owa Hospital during the period between December 2002 and April 2003. Type 2 diabetes was diagnosed on the basis of an abnormal glucose tolerance test result, classic symptoms, and laboratory findings. The inclusion criteria for this study were type 2 diabetes diagnosed at the age of over 30 years and duration of diabetes for more than 2 years. Among 64 type 2 diabetic men, 20 were treated by diet only, 25 with oral medication, and 19 with insulin, and among 81 type 2 diabetic women, 25 were treated by diet only, 22 with oral medication and 34 with insulin. No patient had a history of ketosis and no patient had diabetic retinopathy, nephropathy or peripheral neuropathy.

The non-diabetic healthy control subjects were 41 Japanese men and 54 women (Table 1) and were selected from patients attending the clinic of Rakuwakai Otowa Hospital for their annual medical checkups during the same period. The diabetic patients and the control subjects were similar with regard to physical activity.

All subjects were interviewed by the doctor or nurse and underwent laboratory blood tests. We excluded the subjects who had a history of any fractures and other diseases (liver disease, renal dysfunction, malignancy, hyperthyroidism, hyperparathyroidism, hypercorticoidism, or hypogonadism) and those who had a history of taking medications (active vitamin D3, bisphosphonates, calcitonin injection, estrogens, steroids, thyroid hormone, diuretics, heparin or anticonvulsants) that could influence bone metabolism. All the subjects were subjected to plain X-ray (anteroposterior and lateral views) for the lumbar spine, and patients with scoliosis, compression fractures or ectopic calcifications that could interfere with the bone mineral results were excluded. No subjects were smokers or alcoholics. All subjects gave informed consent.

BMD measurements

BMD was measured at the lumbar spine (L2–L4), the femoral neck, and the distal radius, by DXA (Hologic QDR 4500c, Hologic, Waltham, Mass., USA). To eliminate technical variation, the same operator measured all the subjects. Values of BMD at the lumbar spine were presented as the mean of those at L2–L4. T scores and Z scores were calculated on the basis of the normal reference values of the age- and gender-matched Japanese group provided by the DXA system manufacturer.

Biochemical measurements

Serum calcium, phosphate, creatinine and fasting plasma glucose (FPG) were measured by routine methods. In the type 2 diabetic patients, plasma HbA1c was measured by the latex agglutination method (Fuji Rebio, Tokyo, Japan) and was presented as the mean of several values during the last 2 years before BMD measurement. In diabetic patients treated by diet only or with oral medications (i.e., 45 diabetic men and 47 diabetic women), serum immunoreactive insulin (IRI) was measured by immunoradiometric assay (BML, Kawagoe, Japan) after overnight fasting, and urinary connecting peptide immunoreactivity (CPR) was measured by radioimmunoassay (BML) of the 24-h urine samples collected and stored at −20°C. As markers of bone formation and resorption, serum alkaline phosphatase (ALP) and urinary N-terminal telopeptide of type I collagen normalized by creatinine (NTx/Cre) were measured in diabetic patients and control women. ALP was measured by the routine method (*P*-nitrophenyl-phosphate substrate method). Urinary NTx in the second urine samples in the morning was measured by enzyme-linked immunosorbent assay (BML).

Statistical analysis

Data were analyzed by *t*-test between two group differences, by one-way factorial ANOVA and Fisher's protected least significant difference (PLSD) method among three group differences, and by Pearson's correlation test for examining correlation. Statistics were calculated with

Table 1 Means ± SD of the variables assessed in examined subjects (N.D. not done)

Variable	Men		Women	
	Diabetic patients ($n=64$)	Control subjects ($n=41$)	Diabetic patients ($n=81$)	Control subjects ($n=54$)
Age (years)	62.8 ± 12.0^{NS}	62.9 ± 11.3	66.6 ± 11.4^{NS}	66.1 ± 11.8
BMI (kg/m^2)	23.6 ± 3.6^{NS}	23.1 ± 2.5	23.6 ± 4.6^{NS}	23.2 ± 3.1
Creatinine (mg/dl)	0.75 ± 0.2^{NS}	0.72 ± 0.2	0.63 ± 0.2^{NS}	0.63 ± 0.2
Calcium (mg/dl)	9.2 ± 0.3^{NS}	9.3 ± 0.3	9.2 ± 0.4^{NS}	9.3 ± 0.5
Phosphate (mg/dl)	3.3 ± 0.7^{NS}	3.4 ± 0.6	3.5 ± 0.7^{NS}	3.4 ± 0.6
Urinary NTx/Cre (nmol BCE/mmol Cre)	38.8 ± 11.7	N.D.	44.9 ± 18.6^{NS}	50.6 ± 19.3
ALP (IU/l)	229.0 ± 57.7	N.D.	245.8 ± 66.5^{NS}	234.4 ± 66.5
IRI (μU/ml)	7.0 ± 3.6	N.D.	6.4 ± 3.6	N.D.
Urinary CPR (μg/day)	62.8 ± 42.3	N.D.	45.2 ± 32.6	N.D.
FPG (mg/dl)	$153.7 \pm 46.6^{\dagger}$	90.8 ± 5.3	$155.5 \pm 62.4^{\dagger}$	91.2 ± 5.5
Mean HbA1c (%)	7.8 ± 1.6	N.D.	7.6 ± 1.6	N.D.

P values for comparisons between patients with type 2 diabetes mellitus and control subjects: $^{NS}P > 0.05$, $^{\dagger}P < 0.01$

Statview version 4.0 (Abacus Concepts, Berkeley, Calif., USA). A P value <0.05 was considered as statistically significant.

Results

Table 1 shows a comparison between type 2 diabetic patients and control subjects. There was no significant difference between the two groups in age, BMI and the biochemical parameters except FPG. Among the three diabetic subgroups treated in different ways: diet only, oral medication, and insulin, there was also no significant difference in age, BMI and the mean HbA1c as well as the number of each subgroup (data not shown).

Table 2 and Fig. 1A show a comparison of BMD, T score and Z score between type 2 diabetic patients and control subjects. BMD, T score and Z score at the distal radius were significantly lower in type 2 diabetic patients than in control subjects but were not different at the lumbar spine and the femoral neck, although the Z score at the lumbar spine was significantly higher in type 2 diabetic women. Among the three diabetic subgroups with different treatments, there was no significant difference in BMD, T score and Z score at the three sites (data not shown).

Figure 1B shows a comparison of Z scores at different sites in type 2 diabetic patients, analyzed by one-way factorial ANOVA and Fisher's PLSD test. Z score at the distal radius was significantly lower than those at the lumbar spine and the femoral neck in both men and women, and at the lumbar spine it was significantly higher than that at the femoral neck in women, but not in men.

Table 3 shows correlations of BMD with age, BMI and the biochemical parameters in type 2 diabetic patients. However, correlations of BMD with IRI and urinary CPR were calculated only in type 2 diabetic patients treated by diet only or with oral medications (i.e., 45 diabetic men and 47 diabetic women) because those two parameters were not measured in our insulin-treated patients, as mentioned above. BMDs at the three sites in both genders were associated negatively with age and positively with BMI, except BMD at the distal

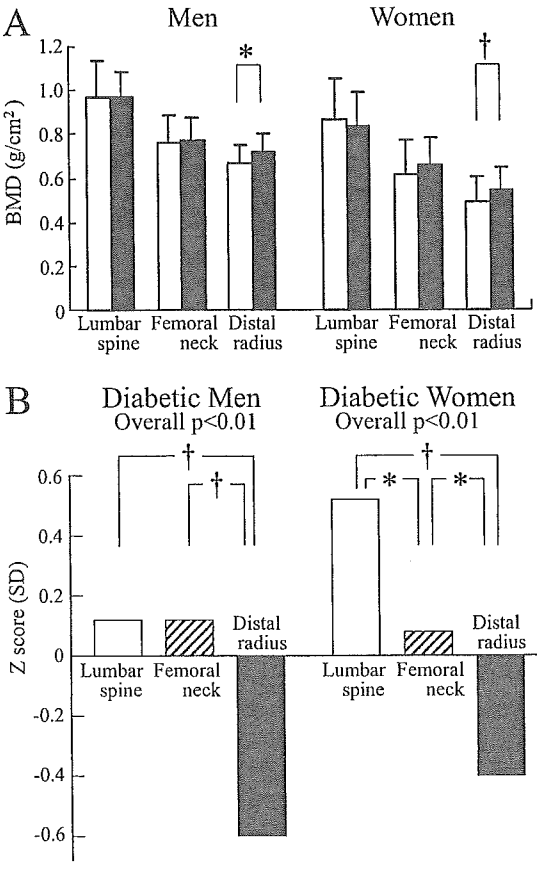

Fig. 1 **A** Comparison of BMDs at the lumbar spine, the femoral neck and the distal radius between patients with type 2 diabetes mellitus (*open columns*) and control subjects (*closed columns*). Each column represents the mean ± SD. $*P<0.05$, $\dagger P<0.01$. **B** Comparison of Z scores at the lumbar spine (*open columns*), the femoral neck (*shaded columns*) and the distal radius (*closed columns*) in patients with type 2 diabetes mellitus. Each column represents the mean value. $*P<0.05$, $\dagger P<0.01$

Table 2 BMD, T score and Z score at the lumbar spine, the femoral neck and the distal radius in type 2 diabetic patients and control subjects. Values are means ± SD

Parameter	Men		Women	
	Diabetic patients	Control subjects	Diabetic patients	Control subjects
Lumbar spine				
BMD (g/cm²)	0.972 ± 0.176^{NS}	0.975 ± 0.108	0.861 ± 0.193^{NS}	0.831 ± 0.162
T score (SD)	-0.640 ± 1.481^{NS}	-0.614 ± 0.905	-1.259 ± 1.618^{NS}	-1.509 ± 1.360
Z score (SD)	0.120 ± 1.005^{NS}	0.096 ± 0.595	$0.533 \pm 1.175^{\dagger}$	0.025 ± 0.979
Femoral neck				
BMD (g/cm²)	0.759 ± 0.137^{NS}	0.767 ± 0.108	0.620 ± 0.153^{NS}	0.660 ± 0.118
T score (SD)	0.820 ± 1.083^{NS}	0.755 ± 0.723	-1.533 ± 1.408^{NS}	-1.167 ± 1.079
Z score (SD)	0.118 ± 1.049^{NS}	0.087 ± 0.787	0.087 ± 1.320^{NS}	0.152 ± 1.075
Distal radius				
BMD (g/cm²)	$0.665 \pm 0.092^{*}$	0.721 ± 0.080	$0.493 \pm 0.109^{\dagger}$	0.547 ± 0.095
T score (SD)	$-1.287 \pm 1.311^{*}$	-0.492 ± 1.144	$-3.321 \pm 2.131^{\dagger}$	-2.257 ± 1.858
Z score (SD)	$-0.610 \pm 1.101^{\dagger}$	0.044 ± 1.014	$-0.397 \pm 1.583^{*}$	0.175 ± 1.224

P-values for comparisons between type 2 diabetic patients and control subjects: $^{NS}P>0.05$, $^{*}P<0.05$, $^{\dagger}P<0.01$

Table 3 Correlations of BMD with age, BMI and the biochemical parameters in type 2 diabetic patients. Values are correlation coefficients. IRI immunoreactive insulin, CPR connecting peptide immunoreactivity, FPG fasting plasma glucose

Parameter	BMD					
	Men			Women		
	Lumbar spine	Femoral neck	Distal radius	Lumbar spine	Femoral neck	Distal radius
Age	−0.310*	−0.519†	−0.409†	−0.409†	−0.575†	−0.692†
BMI	0.375†	0.435†	0.224^{NS}	0.365†	0.493†	0.438†
Creatinine	0.156^{NS}	−0.019^{NS}	−0.034^{NS}	0.130^{NS}	0.049^{NS}	0.042^{NS}
Calcium	0.047^{NS}	0.051^{NS}	0.200^{NS}	0.107^{NS}	0.005^{NS}	0.267^{NS}
Phosphate	0.051^{NS}	−0.065^{NS}	0.079^{NS}	−0.158^{NS}	−0.136^{NS}	−0.166^{NS}
Urinary NTx/Cre	−0.346†	−0.247*	−0.127^{NS}	−0.303*	−0.215^{NS}	−0.258*
ALP	−0.140^{NS}	−0.325†	−0.073^{NS}	−0.050^{NS}	−0.137^{NS}	−0.091^{NS}
IRI	0.085^{NS}	0.305*	0.304*	0.394†	0.382†	0.218^{NS}
Urinary CPR	0.108^{NS}	0.296*	0.314*	0.287^{NS}	0.534†	0.488†
FPG	−0.069^{NS}	−0.019^{NS}	0.035^{NS}	0.056^{NS}	−0.137^{NS}	−0.049^{NS}
Mean HbA1c	−0.182^{NS}	−0.240^{NS}	−0.289*	−0.032^{NS}	−0.314†	−0.219*

P values for correlations of BMD with age, BMI and the biochemical parameters in type 2 diabetic patients: $^{NS}P > 0.05$, $*P < 0.05$, † $P < 0.01$

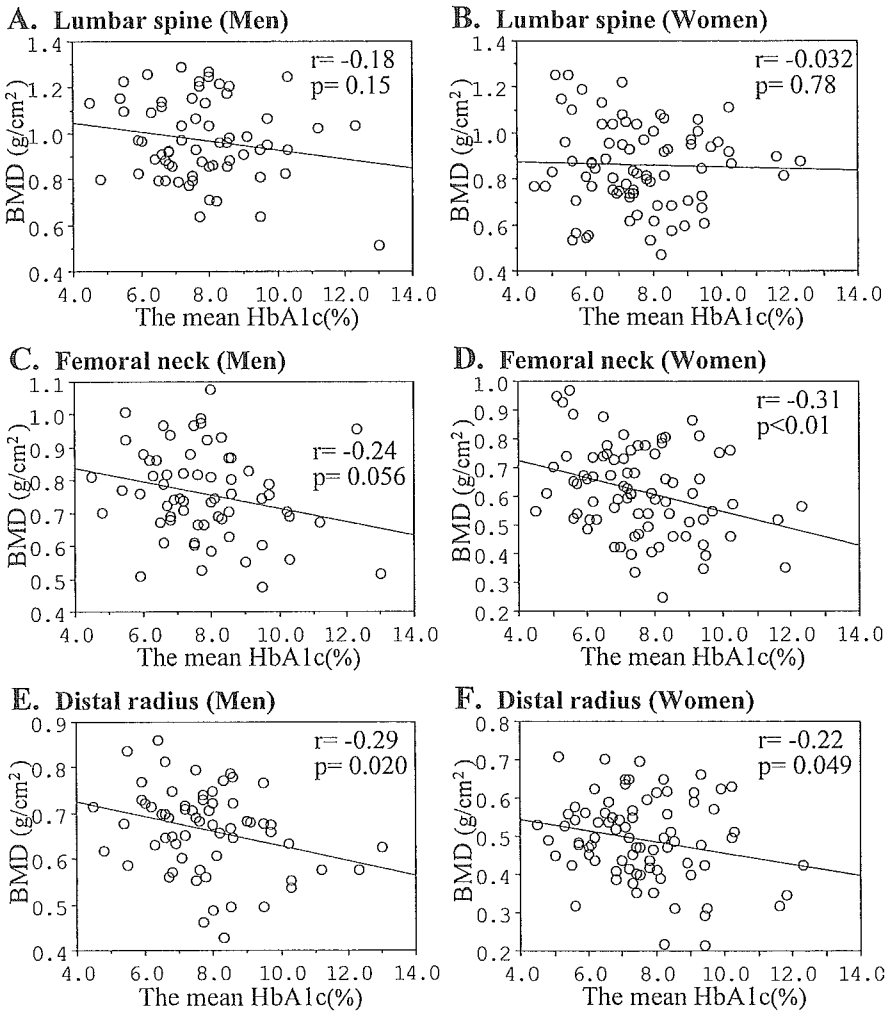

Fig. 2A–F Correlation between the mean HbA1c and BMD at the three sites: lumbar spine (**A**, **B**), femoral neck (**C**, **D**) and distal radius (**E**, **F**) in diabetic men (**A**, **C**, **E**) and diabetic women (**B**, **D**, **F**). For each figure the BMD measurements at each site were plotted against the mean HbA1c levels *The line* reflects the regression and *r* mean correlation coefficients and *P* values for correlations between the mean HbA1c and BMD at the three sites

radius in men with BMI ($P = 0.0754$). Urinary NTx/Cr was negatively correlated with BMD at the lumbar spine in both genders, at the femoral neck in men, and at the distal radius in women. ALP was not correlated with BMD, except at the femoral neck in men. IRI was positively correlated with BMD at the lumbar spine in women, at the femoral neck in both genders, and at the distal radius in men. Urinary CPR was positively

correlated with BMD at the femoral neck and the distal radius in both genders. FPG was not correlated with BMD at any site. The mean HbA1c was negatively correlated with BMD at the femoral neck in women and at the distal radius in both genders (Fig. 2D, E, F), and there was a tendency of negative correlation of the mean HbA1c with BMD at the lumbar spine and at the femoral neck in men (Fig. 2A, C).

Discussion

Our study revealed that BMD of type 2 diabetic patients was significantly lower at the distal radius, but not different at the lumbar spine and the femoral neck, than that of control subjects. and our new finding was that the Z score was the lowest at the distal radius among the three sites (lumbar spine, femoral neck and distal radius) in type 2 diabetic patients. Our results showed that the higher the cortical/cancellous bone ratio (distal radius > femoral neck > lumbar spine), the lower the Z-score became (lumbar spine > femoral neck > distal radius) in type 2 diabetic women. These results suggest that the rapid loss of cortical bone rather than cancellous bone may occur in type 2 diabetes.

Christensen and Svendsen also reported the difference in Z scores among the three sites (lumbar spine > femur total > distal radius) shown in the present study [6]. They examined the BMD of type 2 diabetic women by DXA, but they did not show the statistical significance among the three sites. Leite Duarte and da Silva [22] reported reduced cortical thickness of bone biopsy samples in type 2 diabetic patients. Those results are compatible with our results, suggesting a selective cortical bone loss in type 2 diabetes.

There seem to be many reasons why BMD and Z score at the distal radius were lower in Japanese type 2 diabetic patients in our study, although those at the lumbar spine and femoral neck were higher or not different. The results of the previous studies about BMD of type 2 diabetes were controversial [1, 2, 3, 4, 5, 6, 7, 8, 9, 10, 11, 12, 14, 15]. The different insulin levels in type 2 diabetic patients, high in newly onset cases, low in long-standing cases, might be one of the explanations for the contradictory results of the previous studies [3, 11, 18]. Many previous studies and our present study showed a positive correlation of insulin levels with BMDs [16, 17, 18, 19], because insulin has an anabolic effect on bone [23]. Moreover, Haffner and Bauer [16] and Stolk et al. [18] reported that there was a difference between the association of insulin level with BMD at the lumbar spine and at the femur. Also, our results revealed a difference in the association of insulin level with BMD at the three sites. These results might imply a different effect of insulin on cortical bone from cancellous bone. Therefore, Japanese type 2 diabetic patients with low insulin secretion may have the risk of losing cortical bone and have lower BMDs, especially at the distal radius.

The association between BMDs and insulin levels may be the result of the association between BMD and some other osteogenic factors related to insulin: amylin, estrogen, testosterone, and sex hormone-binding globulin (SHBG). Amylin, which is co-secreted with insulin by the pancreatic β cells in response to glucose load, inhibits bone resorption [24] and increases bone formation [24, 25, 26]. Sex steroids, including estrogen and testosterone, are correlated with insulin levels [7, 18, 27], inhibit bone resorption and increase BMD [28, 29]. Low SHBG levels are correlated with high insulin levels [27, 30] and lead to high sex hormone levels, causing increased BMD [17, 31]. In our study, BMI was strongly correlated with insulin levels, both in men and women with type 2 diabetes ($r=0.454$ $P=0.0018$, $r=0.467$ $P=0.0018$, respectively), as reported in the previous studies [3, 17]. Those insulin-related factors may have influenced bone metabolism and caused the difference in association of insulin levels with BMDs at the three sites in our study.

In the present study, the mean HbA1c was negatively correlated with BMD at the femoral neck in women and the distal radius in both genders, but not at the lumbar spine. Therefore, the association of the mean HbA1c with BMD in the present study seems to be different by the cortical/cancellous bone ratio. This difference may have caused the difference of Z score among the three sites in our study.

Higher BMD associated with poor metabolic control in type 2 diabetic patients [3, 6, 7, 8, 10, 11, 12, 13] could be explained by their hyperinsulinemia, as stated by Stolk et al. in their own study [18]. However, on the other hand, in Japanese type 2 diabetic patients their insulin secretion is not high enough to catch up with increased glucose levels [20, 21]. Therefore, poor metabolic control was not associated with hyperinsulinemia, and so did not lead to higher BMD in our study. Krakauer et al. [1] and Gregorio et al. [14] reported that BMD was decreased in the poorly controlled type 2 diabetic patients and that it was increased by improving metabolic control. Some in vitro studies showed that exposure to high glucose impaired the activity of osteoblasts [32] and stimulated osteoclasts [33]. Those results are in agreement with our results, suggesting that metabolic control of type 2 diabetes is important in preventing bone loss as well as other complications.

Higher parathyroid hormone (PTH) secretion, in part by the negative calcium balance in type 2 diabetic patients, might be one of the reasons for the selective cortical bone loss in type 2 diabetes [14, 34]. Although we did not measure serum PTH, serum calcium was not different between the diabetic patients and the controls.

Whether the bone turnover of type 2 diabetes is higher or lower has not reached consensus yet [1, 5, 6, 7, 8, 12, 14, 22, 34, 35]. Some previous studies reported reduced bone formation in bone biopsy samples of type 2 diabetic patients [1, 22], and reduced osteocalcin in type 2 diabetic patients has been repeatedly reported [6, 7, 34]. Those results are interpreted to represent low

bone formation in type 2 diabetes [1, 6, 7, 22, 34]. However, in contrast, ALP and bone type alkaline phosphatase (BAP), other bone formation markers, were reported to be elevated in type 2 diabetes in other previous studies [35, 36], as in our study. This is probably because maturation of osteoblasts is inhibited at the mineralization phase after ALP expression in type 2 diabetes [37]. Therefore, considering that in our study ALP was relatively higher and urinary NTx/Cre was relatively lower in type 2 diabetic women, we consider that type 2 diabetic women in our study had relatively a lower rate of bone turnover than controls. This lower rate of bone turnover may offset rapid bone loss with high bone turnover during perimenopausal period [1, 3, 6], especially at the lumbar spine. Therefore, type 2 diabetic women in the present study might not have lost bone at the lumbar spine, and so their BMD at the lumbar spine might have become higher than that of control women and also than their own BMDs at the other sites.

From these observations, it can be seen that cortical bone and cancellous bone could be differently affected by the conditions of type 2 diabetes, including insulin, glucose, BMI, sex steroids and PTH. However, further studies are needed to clarify these issues.

In conclusion, we found that BMD at the distal radius was significantly decreased in type 2 diabetic patients compared with controls and that Z score at the radius was significantly lower than that at their own lumbar spine and their own femoral neck in type 2 diabetic patients. In addition, we found negative correlation of the mean HbA1c during the previous 2 years with BMD at the femoral neck and the distal radius, but not at the lumbar spine, in type 2 diabetic patients. These results suggest a selective cortical bone loss in type 2 diabetes. Therefore, we conclude that it is important to determine BMD at the radius as well and that good metabolic control leads to prevention of bone loss in type 2 diabetic patients.

Acknowledgement This work is supported by grants from Research for the Future of the Japan Society for the Promotion of Science; the Japanese Ministry of Education, Sciences, Sports, and Culture; Smoking Research Foundation and Foundation for Growth Science.

References

1. Krakauer JC, McKenna MJ, Buderer NF, Rao DS, Whitehouse FW, Parfitt AM (1995) Bone loss and bone turnover in diabetes. Diabetes 44:775–782
2. Tuominen JT, Impivaara O, Puukka P, Ronnemaa T (1999) Bone mineral density in patients with type 1 and type 2 diabetes. Diabetes Care 22:1196–1200
3. Barrett-Connor E, Holbrook TL (1992) Sex differences in osteoporosis in older adults with non-insulin-dependent diabetes mellitus. JAMA 16:3333–3337
4. Wakasugi M, Wakao R, Tawata M, Gan N, Koizumi K, Onaya T (1993) Bone mineral density by dual energy X-ray absorptiometry in patients with non-insulin-dependent diabetes mellitus. Bone 14:29–33
5. Sosa M, Dominquez M, Navarro MC, Segarra MC, Hernandez D, de Pablos P, Betancor P (1996) Bone mineral metabolism is normal in non-insulin-dependent diabetes mellitus. J Diabetes Complications 10:201–205
6. Christensen JO, Svendsen OL (1999) Bone mineral in pre- and postmenopausal women with insulin-dependent and non-insulin-dependent diabetes mellitus. Osteoporos Int 10:307–311
7. el Miedany YM, el Gaafary S, el Baddini MA (1999) Osteoporosis in older adults with non-insulin-dependent diabetes mellitus: is it sex related? Clin Exp Rheumatol 17:561–567
8. Isaia GC, Ardissone P, Di Stefano M, Ferrari D, Martina V, Porta M, Tagliabue M, Molinatti GM (1999) Bone metabolism in type 2 diabetes mellitus. Acta Diabetol 36:35–38
9. Bartos V, Jirkovska A, Kasalicky P, Smahelova A, Vondra K, Skibova J (2001) Osteopenia and osteoporosis in diabetic women over 40 years of age. Cas Lek Cesk 140:299–301
10. Sert M, Tetiker T, Kirim S, Soyupak S, Canataroglu A, Kocak M (2003) Type 2 diabetes mellitus and osteopenia: is there an association? Acta Diabetol 40:105–108
11. van Daele PL, Stolk RP, Burger H, Algra D, Grobbee DE, Hofman A, Birkenhager JC, Pols HA (1995) Bone density in non-insulin-dependent diabetes mellitus: the Rotterdam Study. Ann Intern Med 122:409–414
12. Sahin G, Bagis S, Cimen OB, Ozisik S, Guler H, Erdogan C (2001) Lumbar and femoral bone mineral density in type 2 Turkish diabetic patients. Acta Medica (Hradec Kralove) 44:141–143
13. Akin O, Gol K, Akturk M, Erkaya S (2003) Evaluation of bone turnover in postmenopausal type 2 diabetic patients using biochemical markers and bone mineral density measurements. Gynecol Endocrinol 17:19–29
14. Gregorio F, Cristallini S, Santeusanio F, Filipponi P, Fumelli P (1994) Osteopenia associated with non-insulin-dependent diabetes mellitus: what are the causes? Diabetes Res Clin Pract 23:43–54
15. Levin ME, Boisseau VC, Avioli LV (1976) Effects of diabetes mellitus on bone mass in juvenile and adult-onset diabetes. N Engl J Med 294:241–245
16. Haffner SM, Bauer RL (1993) The association of obesity and glucose and insulin concentrations with bone density in premenopausal and postmenopausal women. Metabolism 42:735–738
17. Reid IR, Evans MC, Cooper GJ, Ames RW, Stapleton J (1993) Circulating insulin levels are related to bone density in normal postmenopausal women. Am J Physiol 265:E655–659
18. Stolk RP, van Daele PL, Pols HA, Burger H, Hofman A, Birkenhager JC, Lamberts SW, Grobbee DE (1996) Hyperinsulinemia and bone mineral density in an elderly population: The Rotterdam Study. Bone 18:545–549
19. Barrett-Connor E, Kritz-Silverstein D (1996) Does hyperinsulinemia preserve bone? Diabetes Care 19:1388–1392
20. Akanuma Y (1996) Non-insulin-dependent diabetes mellitus (NIDDM) in Japan. Diabet Med 13:S11–S12
21. Yoshinaga H, Kosaka K (1999) Heterogeneous relationship of early insulin response and fasting insulin level with development of non-insulin-dependent diabetes mellitus in non-diabetic Japanese subjects with or without obesity. Diabetes Res Clin Pract 44:129–136
22. Leite Duarte ME, da Silva RD (1996) Histomorphometric analysis of the bone tissue in patients with non-insulin-dependent diabetes (DMNID). Rev Hosp Clin Fac Med Sao Paulo 51:7–11
23. Yano H, Ohya K, Amagasa T (1996) Insulin enhancement of in vitro wound healing in fetal rat parietal bones. J Oral Maxillofac Surg 54:182–186
24. Cornish J, Callon KE, Cooper GJ, Reid IR (1995) Amylin stimulates osteoblast proliferation and increases mineralized bone volume in adult mice. Biochem Biophys Res Commun 207:133–139
25. Mitsukawa T, Takemura J, Asai J, Nakazato M, Kangawa K, Matsuo H, Matsukura S (1990) Islet amyloid polypeptide response to glucose, insulin, and somatostatin analogue administration. Diabetes 39:639–642

26. Hartter E, Svoboda T, Ludvik B, Schuller M, Lell B, Kuenburg E, Brunnbauer M, Woloszczuk W, Prager R (1991) Basal and stimulated plasma levels of pancreatic amylin indicate its cosecretion with insulin in humans. Diabetologia 34:52–54
27. Khaw KT, Barrett-Connor E (1991) Fasting plasma glucose levels and endogenous androgens in non-diabetic postmenopausal women. Clin Sci (Lond) 80:199–203
28. Riis BJ, Overgaard K, Christiansen C (1995) Biochemical markers of bone turnover to monitor the bone response to postmenopausal hormone replacement therapy. Osteoporos Int 5:276–280
29. Anderson FH, Francis RM, Faulkner K (1996) Androgen supplementation in eugonadal men with osteoporosis—effects of 6 months of treatment on bone mineral density and cardiovascular risk factors. Bone 18:171–177
30. Nestler JE (1993) Sex hormone-binding globulin: a marker for hyperinsulinemia and/or insulin resistance? J Clin Endocrinol Metab 76:273–274
31. van Hemert AM, Birkenhager JC, De Jong FH, Vandenbroucke JP, Valkenburg HA (1989) Sex hormone binding globulin in postmenopausal women: a predictor of osteoporosis superior to endogenous oestrogens. Clin Endocrinol (Oxf) 31:499–509
32. Balint E, Szabo P, Marshall CF, Sprague SM (2001) Glucose-induced inhibition of in vitro bone mineralization. Bone 28:21–28
33. Williams JP, Blair HC, McDonald JM, McKenna MA, Jordan SE, Williford J, Hardy RW (1997) Regulation of osteoclastic bone resorption by glucose. Biochem Biophys Res Commun 235:646–651
34. Nagasaka S, Murakami T, Uchikawa T, Ishikawa SE, Saito T (1995) Effect of glycemic control on calcium and phosphorus handling and parathyroid hormone level in patients with non-insulin-dependent diabetes mellitus. Endocr J 42:377–383
35. Okazaki R, Totsuka Y, Hamano K, Ajima M, Miura M, Hirota Y, Hata K, Fukumoto S, Matsumoto T (1997) Metabolic improvement of poorly controlled noninsulin-dependent diabetes mellitus decreases bone turnover. J Clin Endocrinol Metab 82:2915–2920
36. Stepan J, Havranek T, Formankova J, Skrha J, Skrha F, Pacovsky V (1980) Bone isoenzyme of serum alkaline phosphatase in diabetes mellitus. Clin Chim Acta 105:75–81
37. Stein GS, Lian JB (1993) Molecular mechanisms mediating proliferation/differentiation interrelationships during progressive development of the osteoblast phenotype. Endocr Rev 14:424–442

Endocrine Journal 2005, **52** (5), 551–557

Anaplastic Thyroid Carcinoma Associated with Graves' Disease

TAKAFUMI MAJIMA*,**, YASATO KOMATSU**, KENTARO DOI*, MICHIKA SHIGEMOTO*, CHIEKO TAKAGI*, ATSUSHI FUKAO***, MASATSUGU KOJIMA#, HISANOBU TAMAKI#, JUICHI ITO# AND KAZUWA NAKAO**

**Department of Endocrinology and Metabolism, Rakuwakai Otowa Hospital, Kyoto 607-8062, Japan*
***Department of Medicine and Clinical Science, Kyoto University Graduate School of Medicine, Kyoto 606-8507, Japan*
****Department of Psychosomatic Medicine, Rakuwakai Otowa Hospital, Kyoto 607-8062, Japan*
#Department of Otolaryngology - Head and Neck Surgery, Graduate School of Medicine, Kyoto University, Kyoto 606-8507, Japan

Abstract. This report concerns a 79-year-old woman with coexisting anaplastic thyroid carcinoma (ATC) and Graves' disease (GD). The patient was referred to our clinic because of palpitation and a palpable mass on the left side of her neck. Thyroid function tests showed hyperthyroidism with elevated thyroid-stimulating antibodies. Ultrasonography of the thyroid demonstrated an adenomatous nodule-like marcated nodule (27.6 × 26.5 × 36.4 mm) with cystic degeneration inside the left lobe. ^{123}I thyroid scintigraphic imaging showed a cold area corresponding to the nodule with continuous uptake in the remaining thyroid tissue despite suppressed TSH levels. These findings led to a diagnosis of GD. On the other hand, the thyroid nodule could not be definitely diagnosed even after fine needle aspiration biopsy (FNAB) which produced findings suggestive of both papillary thyroid carcinoma and ATC. Open biopsy of the nodule showed an ATC. Regional lymph node metastases as well as multiple lung metastases, which could not be found at the initial visit, had been already developed by that time. Our case is pathophysiologically interesting because it suggests that GD or thyroid-stimulating antibodies (TSAb) may stimulate malignant transformation of differentiated carcinoma. It is also clinically important because it indicates that all thyroid nodules, particularly palpable cold nodules, associated with GD require careful management to detect malignancy because they are at higher risk of harboring malignancy.

Key words: Anaplastic thyroid carcinoma, Graves' disease, Thyroid-stimulating antibody, Anaplastic transformation
(*Endocrine Journal* **52**: 551–557, 2005)

THYROID nodules occur commonly in association with Graves' disease (GD) and more frequently than in the general population [1, 2]. Since 2.3% to 45.8% of these nodules accompanying GD have been reported to be malignant [1, 2] and the aggravated aggressiveness of thyroid cancer in GD has been described in numerous reports [3–9], the presence of thyroid nodules in conjunction with GD should cause concern about coexistent thyroid malignancy. However, how to preoperatively diagnose malignancy in GD-associated nodules with certainty has not yet been fully established [2, 10–13].

On the other hand, anaplastic thyroid carcinoma (ATC) is not common, accounting for only about 2% of all thyroid carcinomas, but it is one of the most aggressive malignant diseases with very poor prognosis [14, 15]. To the best of our knowledge, only six case reports, including the one presented here, on ATC associated with hyperthyroidism have ever been published [3, 4, 16, 17], and whether GD affects the initiation, promotion or prognosis of ANA remains obscure.

In this report, we present a rare case of ATC associated with GD.

Received: March 23, 2005
Accepted: May 16, 2005
Correspondence to: Takafumi MAJIMA, M.D., Department of Endocrinology and Metabolism, Rakuwakai Otowa Hospital, 2 Otowa Chinji-cho, Yamashina-ku, Kyoto 607-8062, Japan

Case Report

A 79-year-old Japanese woman was first referred to the Otowa Clinic in March 2004 because of palpitation, weight loss, and a painless mass on the left side of the neck. She had noticed the enlarged neck mass a few weeks earlier, but did not complain of compressive neck symptoms, dysphagia, hoarseness, or shortness of breath. She had lost 3 kg of body weight (from 51 kg to 48 kg) without loss of appetite over the previous 3 months. Other signs or symptoms suggestive of hyperthyroidism were not present. She had neither a family history of thyroid diseases nor a past history of radiation of the head or neck.

Physical examination showed her blood pressure and pulse to be normal. A golfball-sized, painless, and rather hard mass (approximately 4 cm in diameter) with a smooth surface was palpated on the anterior left side of the neck. No lymph nodes were palpable in the neck or supraclavicular region and other physical examination results were unremarkable.

Ultrasonography of the thyroid showed a marcated nodule containing cystic degeneration and measuring 27.6 × 26.5 × 36.4 mm (Fig. 1). Neck computed tomography (CT) scan showed some tracheal deviation to the right without narrowing of the airway, but neither of these imaging procedures produced any remarkable findings in the right thyroid lobe or lymph node swellings.

Routine laboratory data showed no abnormalities (CRP <0.24 mg/dl) except a somewhat elevated WBC 8100/μl with a slight increase in the neutrophil ratio (65.3%) and a decreased lymphocyte ratio (27.2%). However, thyroid function tests showed elevated free triiodothyronine (T3) of 4.88 pg/ml (reference range: 2.30–4.30 pg/ml) and free thyroxine (T4) of 2.53 ng/dl (reference range: 0.90–1.70 ng/dl), and virtually undetectable thyroid-stimulating hormone (TSH) at <0.005 μIU/ml (reference range: 0.500–5.00 μIU/ml). Serum thyroglobulin was 140.6 ng/ml (reference range: <30 ng/ml), and thyroid-stimulating antibody (TSAb), TSH receptor antibodies (TRAb), anti-thyroglobulin (TgAb) and anti-thyroperoxidase (TPOAb) antibodies were all elevated at 203.0% (reference range: <180%), 42.4% (reference range: <15%), 2.00 U/ml (reference range: <0.3 U/ml), and 73.3 U/ml (reference range: <0.3 U/ml), respectively.

A thyroid iodine-123 (^{123}I) scintigram after an iodine restricted diet for 7 days showed a cold area corresponding to the thyroid nodule, with maintained uptake in the remaining thyroid tissue although TSH was reduced to below the level of sensitivity (Fig. 2). Three-hour and 24-hour radioactive iodine thyroid uptakes were 5.63% (reference range: 5–15%) and 29.61% (reference range: 10–40%), respectively, although compliance with the restricted diet could not be assured because she was instructed as an outpatient at her request.

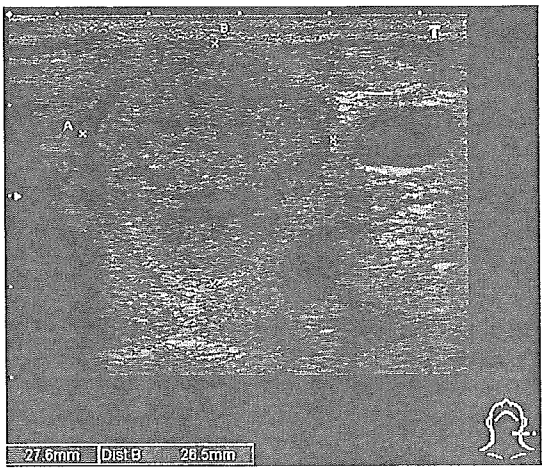

A

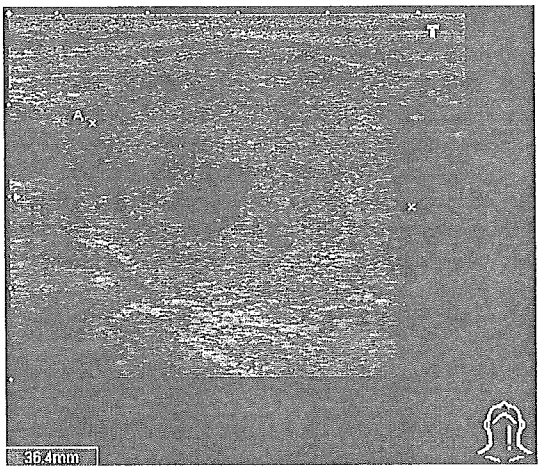

B

Fig. 1. Ultrasonography of the left thyroid lobe. (A) Horizontal section. (B) Sagittal section.

Our diagnosis was hyperthyroidism resulting from GD, and we began treating it with an anti-thyroid drug (methimazole, 15 mg/day). Since the nodule could not be diagnosed, however, we recommended fine needle aspiration biopsy (FNAB) to determine whether the nodule was malignant or not, but she refused and

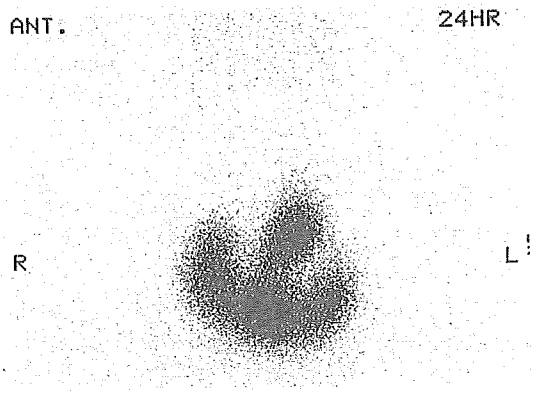

Fig. 2. Thyroid ^{123}I scintigram demonstrating a cold area corresponding to the thyoid nodule in the left lobe. The rest of the gland shows maintained uptake despite TSH suppressed below sensitivity.

stopped coming to our clinic. Instead, she attended the department of otorhinolaryngology of Kyoto University Hospital, where FNAB of the nodule was performed on 24 June 2004, showing Papanicolaou V. Atypical cells were found in biopsy specimens from the nodule, some of which had large nuclei with a pale ground-glass appearance or with intranuclear inclusion. Although the nodule could be interpreted as a papillary adenocarcinoma, the degree of pleomorphism was substantially higher than that generally seen in association with a differentiated carcinoma, and the atypical cells were isolated from each other, indicating an anaplastic thyroid carcinoma. The results of the FNAB showed the nodule to be malignant, but its histological type could not be diagnosed accurately.

Open biopsy of the nodule was thus performed in July 2004, and microscopic examination found marked pleomorphisms without duct-like configurations anywhere in the nodule. There were numerous giant cells, some of which contained multiple nuclei, against a background of some spindle cells and a scattering of neutrophils (Fig. 3). The nodule was therefore diagnosed as ATC. The biopsied tissue specimens contained only malignant cells and no benign or hyperplastic cells suggestive of GD.

By that time, the nodule had grown into a huge mass incorporating surrounding lymph node swellings, and chest roentgenography and CT showed findings suggesting multiple lung metastases. Furthermore, thyroid function declined to below the reference range without medication, probably because malignant tissue had mostly replaced the thyroid tissue associated with GD

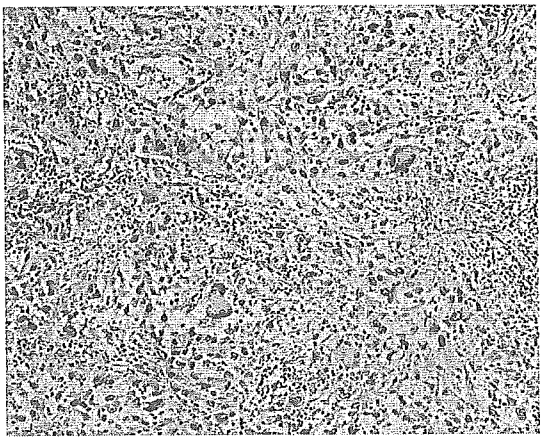

A

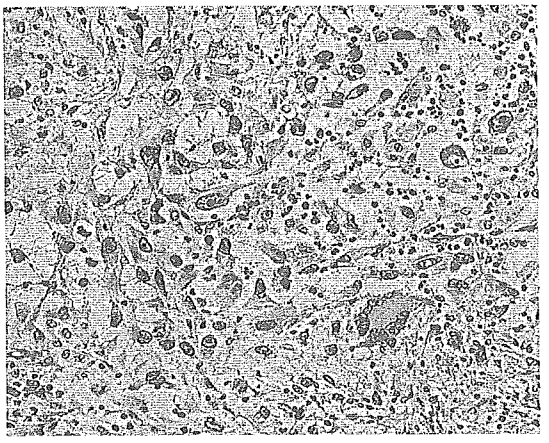

B

Fig. 3. Histologic appearance of the thyroid tumor demonstrating marked pleomorphism without duct-like configuration. There were numerous giant cells, some of which contained multiple nuclei, against a background of some spindle cells and a scattering of neutrophils. (A) Hematoxylin-eosin stain; ×100. (B) Hematoxylin-eosin stain; ×200.

or because TSH binding inhibitor immunogloblins (TBII) might have emerged although not measured, so that the patient needed levothyroxine (L-T4) replacement therapy (75 μg/day). She was diagnosed as no longer curable with surgery, and was treated in vain with oral chemotherapy. In December 2004, she died of respiratory failure probably due to airway narrowing.

Discussion

Our patient with GD presented with a solitary pal-

pable thyroid nodule, which revealed ATC. It has been reported that a palpable thyroid nodule occurs in approximately 12.8% to 26.9% of patients with GD [11, 18–20], and in 33.6% when detected ultrasonographically [21]. This comparatively high frequency of thyroid nodule occurrence has therefore raised clinical concern about the co-existence of thyroid malignancy [11].

The reported frequencies of thyroid cancer in patients with GD are reviewed in Table 1, ranging from 0% to as high as 12.5% [5–13, 18–43]. In comparison, thyroid cancer is an infrequent malignant tumor in the general population, with an incidence ranging from 0.5 to 10 per 100,000 [1]. Furthermore, when a nodule is detected in association with GD, the malignancy rate of the nodule is reportedly 10% to 17.1% [10, 11, 20, 43], and becomes higher if the patient is older [13], or if the nodule is palpable [7, 35, 40], solitary [22], or scintigraphically cold [7, 20, 41, 43] whereas carcinoma in a hot nodule is extremely rare [22, 44]. Therefore, it would appear that the nodule in our case had potentially high risk of malignancy. It is regrettable that our ef-

Talbe 1. Published series of thyroid cancer in patients with Graves' disease

Authors and Year		Patients with GD	Patients with GD with Cancer		Histology of Cancer		
					Papillary	Follicular	Other
		(n)	(n)	(%)	(n)	(n)	(n)
Beahrs *et al.*[23]	51	3029	14	0.46		not shown	
Sokal[24]	54	13868	21	0.15		not shown	
Shaprio *et al.*[25]	70	172	15	8.7	10	10	1
Dobyns *et al.*[18]	74	30343	47	0.15	33	7	7
Hancock *et al.*[26]	77	451	7	1.5	4	3	
Wahl *et al.*[27]	82	178	2	1.1	2		
Farbota *et al.*[28]	85	117	6	5.1	4	2	
Behar *et al.*[5]	86	194	10	5.2		not shown	
Pacini *et al.*[19]	88	86	6	6.9	2	4	
Rieger *et al.*[29]	89	64	0	0.0		0	
Ozaki *et al.*[6]	90	743	19	2.6	15	4	
Belfiore *et al.*[7]	90	132	13	9.8		not shown	
Hales *et al.*[30]	92	886	16	1.8	15	1	
Chou *et al.*[31]	93	674	10	1.5	9	1	
Terzioglu *et al.*[32]	93	33	2	6.1	2		
Soh and Park[33]	93	545	11	2.2	10	1	
Kasuga *et al.*[34]	93	847	36	4.3	30	6	
Thakur *et al.*[35]	95	49	4	8.2	3	1	
Miccoli *et al.*[36]	96	140	13	9.3	13		
Pomorski *et al.*[37]	96	704	3	0.4	1	2	
Carnell and Valente[20]	98	468	6	1.3	5	1	1
Pellegriti *et al.*[8]	98	450	36	8.0		not shown	
Cantalamessa *et al.*[21]	99	315	1	0.32		not shown	
Chao *et al.*[9]	99	2934	30	1.0		not shown	
Vaiana *et al.*[38]	99	108	7	6.4	7		
Ruggieri *et al.*[39]	99	8	1	12.5	1		
Kraimps *et al.*[10]	00	557	21	3.8	20	1	
Mishra and Mishra[11]	01	130	8	6.2	5	1	2
Zanella *et al.*[40]	99	38	2	5.3	1	1	
Stocker *et al.*[41]	02	325	6	1.9	6		
Lin *et al.*[22]	03	42	4	9.5	1	2	1
Gabriele *et al.*[12]	03	64	0	0.0		0	
Gerenova *et al.*[42]	03	103	8	7.8	8		
Chao *et al.*[43]	04	3112	61	2.0	58	1	2
Kim *et al.*[13]	04	245	8	3.3	8		